Journal of Catalysis 365 (2018) 43–54

Contents lists available at ScienceDirect

Journal of Catalysis

journal homepage: www.elsevier.com/locate/jcat

Structural elucidation of supported Rh complexes derived from RhCl$(PPh_3)_3$ immobilized on surface-functionalized SBA-15 and their catalytic performance for C-heteroatom (S, O) bond formation

Yong Yang [a,b,*], Ji Wong Chang [b,d], Robert M. Rioux [b,c,*]

[a] Key CAS Biobased-Materials Laboratory, Qingdao Institute of Bioenergy and Bioprocess Technology, Chinese Academy of Sciences, Qingdao 266101, China
[b] Department of Chemical Engineering, The Pennsylvania State University, University Park, PA 16802, United States
[c] Department of Chemistry, The Pennsylvania State University, University Park, PA 16802, United States
[d] Department of Chemical Engineering, Kumoh National Institute of Technology, Gumi-si, Kyeongsangbuk-do 39177, South Korea

ARTICLE INFO

Article history:
Received 27 April 2018
Revised 6 June 2018
Accepted 11 June 2018

Keywords:
Rhodium
Wilkinson's catalyst
Surface organometallic catalyst
Nuclear magnetic resonance
Extended X-ray absorption spectroscopy
Hydrothiolation
Hydrosulfonation
Stereoselectivity

ABSTRACT

The local structures of rhodium complexes derived from the immobilization of Wilkinson's complex, RhCl$(PPh_3)_3$, on SBA-15 silica functionalized with primary–amine, secondary–amine, or diphenylphosphine groups within the mesoporous channels were characterized by a series of techniques including XRD, HR-TEM, multinuclear ($^{13}C/^{29}Si/^{31}P$) solid-state NMR, 2D $^{31}P\{^1H\}$ HETCOR NMR, XPS, and Rh *K*-edge EXAFS. Immobilization of RhCl$(PPh_3)_3$ through covalent bond formation with different functional groups grafted to the silica surface lead to variations in the local structure of the Rh center that has important implications for catalysis. The immobilized Rh complexes demonstrated high activity for the addition of alkynes with thiols (hydrothiolation) or sulfonic acids (hydrosulfonation) with excellent regio- and stereoselectivity under mild reaction conditions. This work demonstrates the elucidation of the local structure of the immobilized Rh complexes requires a complimentary multi-technique characterization approach that probes both the metal center itself and surrounding ligands.

1. Introduction

The immobilization of catalytically active species, i.e. organometallic complexes, onto a solid support to produce a molecular heterogeneous catalyst is one potential solution to issues associated with homogeneous catalysis, such as catalyst recyclability and separation from the product mixture [1–3]. The merits of heterogeneous catalysts are derived not only from their ease of separation from the reaction media, but also their unique activity derived from their site-isolation and the structure of the surface-bound catalytic active sites.

Functionalization of supports via organic modification provides their surfaces with many favorable properties for various practical applications in gas storage, separation, catalysis, and drug delivery. Immobilization of organometallic complexes through covalent bond formation with functional groups on supports is the most commonly employed method to form heterogenized organometallic catalysts that are applicable for a variety of catalytic chemistries including hydrogenation [4–6], hydroformylation [7–10], and hydrosilylation [12,13]. The chemical bonding between metal complexes and functional groups of the support maintains the isolated nature of metal complexes at dilute surface densities, which can influence the catalytic performance in a manner that the analogous homogeneous complex does not exhibit in solution [14–19]. These grafted structures not only reduce metal leaching from the support and subsequent metal contamination of the products, but in selected examples provide an enhancement in activity and selectivity relative to the analogous homogeneous complex [4–11].

Wilkinson's complex, RhCl$(PPh_3)_3$, is a well-known homogeneous hydrogenation catalyst in organic synthesis and the production of fine chemicals [20–26]. It has been immobilized onto supports using various functional groups to form heterogeneous catalysts which have shown high activity and stability during catalysis [6,27–34]. In spite of tremendous effort dedicated to the immobilization of homogeneous complexes over the last two decades [35], investigations of the local structures of RhCl$(PPh_3)_3$ upon immobilization on surface-functionalized supports especially with

* Corresponding authors at: Key CAS Biobased-Materials Laboratory, Qingdao Institute of Bioenergy and Bioprocess Technology, Chinese Academy of Sciences, Qingdao 266101, China (Y. Yang); Department of Chemical Engineering, The Pennsylvania State University, University Park, PA 16802, United States (R.M. Rioux).

E-mail addresses: yangyong@qibebt.ac.cn (Y. Yang), rioux@engr.psu.edu (R.M. Rioux).

https://doi.org/10.1016/j.jcat.2018.06.012
0021-9517/

emphasis on the correlation of the structures with catalytic activities and/or selectivity are scarce. Possible structures of immobilized Rh species have been proposed previously in the literature [36–38], but these studies have not adequately combine spectroscopic characterization(s) of the heterogeneous species that probe both the grafted metal center and ligand environment. Additionally, the most thorough study to date [36] did not perform catalytic experiments to correlate kinetic behavior with the structure of the grafted organometallic catalyst (i.e. a structure-function relationship). We aim to determine the local structure of immobilized analogs of Wilkinson's catalyst through rigorous spectroscopic characterization in order to establish structure-function relationships for carbon-heteroatom bond formation reactions.

Recently, we reported the highly regio- and stereoselective hydrothiolation of alkynes with thiols to produce valuable vinyl sulfides catalyzed by immobilized Rh complexes with high activity and stability (Scheme 1) [39]. We found the regio- and stereoselectivity for vinyl sulfides is highly dependent on the immobilized Rh complexes derived from the reaction of $RhCl(PPh_3)_3$ with surface-functionalized SBA-15 bearing different functional groups: primary–amine, secondary–amine, and diphenylphosphine. We believe the local structure of the immobilized Rh complexes is primarily responsible for such differences in stereoselectivity, but did not pursue the origin of these stereoselectivity differences in our previous work, which motivated us to determine their exact structure with an in-depth characterization study to reveal the structure-function relationships between activity/selectivity and the Rh center.

In this paper, we elucidate the local structure of immobilized Rh complexes, derived from the reaction of Wilkinson's complex with surface-functionalized SBA-15 by systematic characterization using X-ray diffraction (XRD), physical adsorption, high-resolution transmission electron microscopy (HR-TEM), X-ray photoelectron spectroscopy (XPS), multi-nuclear (^{13}C, ^{29}Si, and ^{31}P) solid-state nuclear magnetic resonance (NMR) spectroscopy, $^{31}P\{^1H\}$ HETCOR (heteronuclear correlation) 2D NMR, and Rh *K*-edge extended X-ray absorption fine structure (EXAFS) spectroscopy. The structure-function relationship between activity/selectivity of the Rh center for alkyne hydrothiolation was clearly disclosed. In addition, we extend the use of such immobilized Rh complexes to C—O bond formation chemistry – the addition of alkynes with sulfonic acids (hydrosulfonation) – to produce valuable vinyl sulfonates, which are important and versatile building blocks in organic synthesis, especially for cross-coupling [40–44], carbonylation [45], and polymerization [46] reactions. They also represent attractive intermediates for the formation of vinyl cations or alkylidiene carbenes [47]. The immobilized Rh complexes demonstrate high activity, excellent regio- and stereoselectivity, broad substrate versatility, and significant stability.

2. Results and discussion

2.1. Preparation and characterization of the catalysts

SBA-15 silica was prepared using a $(EO)_{20}(PO)_{70}(EO)_{20}$ (P123) triblock co-polymer and tetraethyl orthosilicate (TEOS) under acidic conditions according to a previously reported procedure [48]. The immobilized Wilkinson's complex, $RhCl(PPh_3)_3$, on surface-functionalized SBA-15 was prepared under a nitrogen atmosphere in a step-by-step manner as shown in Scheme 1. The functionalized samples were labeled as N-SBA-15 (primary amine, (3-aminopropyl)triethoxysilane)), 2N-SBA-15 (secondary amine, [3-(2-aminoethylamino)-propyl]triethoxysilane)), P-SBA-15 (diphenylphosphine), and the corresponding immobilized catalysts were labeled as Rh-N-SBA-15, Rh-2N-SBA-15, and Rh-P-SBA-15, respectively. A nominal loading of 1 wt% Rh was introduced to each sample, and the Rh loading determined by ICP-AES to be 0.92, 0.89, and 0.91, respectively.

The nitrogen adsorption isotherms of SBA-15, P-SBA-15, and Rh-P-SBA-15 as representative samples, respectively, shown in Fig. S1, displayed typical IV type N_2 adsorption-desorption isotherms with a clear H1 hysteresis loop, indicating the highly ordered mesoporous channel structures of SBA-15 were preserved upon organic functionalization and subsequent immobilization of Wilkinson's complex. The hysteresis loops of SBA-15, P-SBA-15, and Rh-P-SBA-15 gradually shifted to lower relative pressures, especially for Rh-P-SBA-15, indicating a lower relative pressure at which capillary condensation commences and a decrease in surface area. This is consistent with changes in pore size distribution,

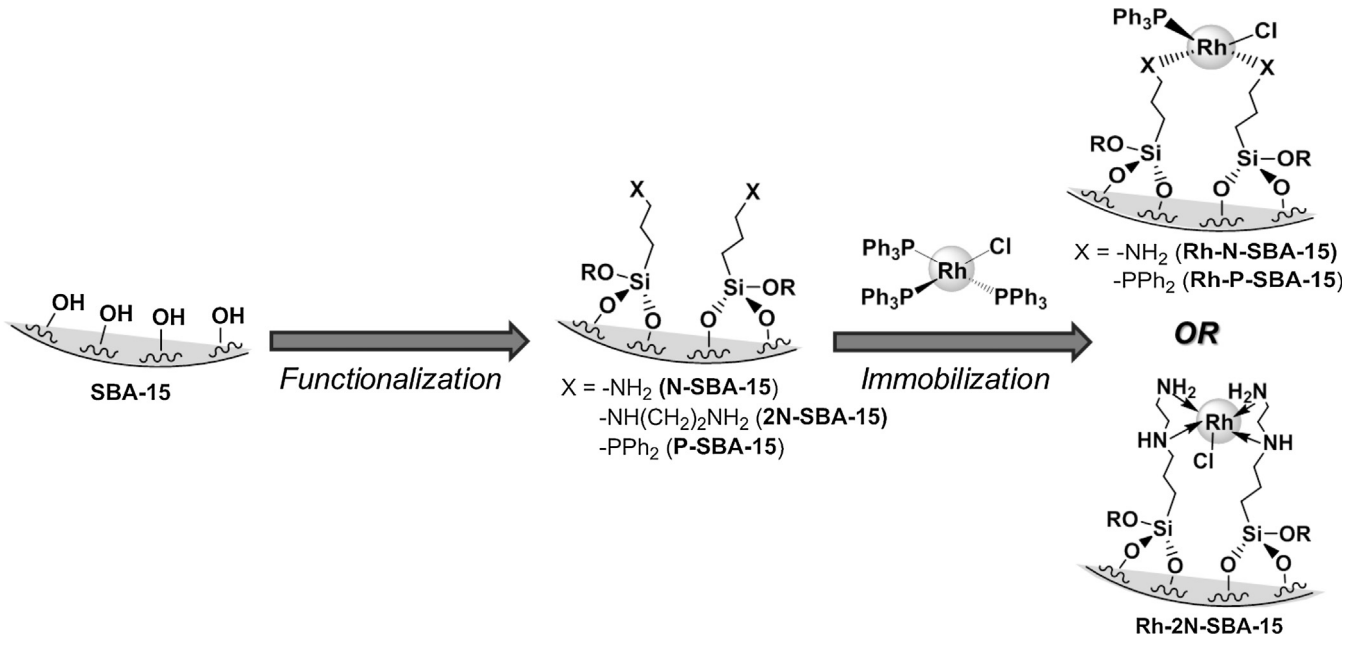

Scheme 1. Preparation of immobilzed Rh complexes on surface-functionalized SBA-15.

as shown in Fig. S1. We observed a similar behavior for the amine-functionalized SBA-15 silica materials.

Functionalization and immobilization of Wilkinson's complex caused a reduction in the surface area, total pore volume, and mean pore size compared with pure SBA-15, as listed in Table S1. The low-angle XRD pattern (Fig. S2) for all samples showed three well-resolved peaks in the region of 0.6–2° indexed to (1 1 0), (2 0 0), and (2 1 1) reflections of hexagonal mesoporous arrays and a significant decrease in their reflection intensities compared with pure SBA-15. A positive shift in peak position for the P-SBA-15 and Rh-P-SBA-15 samples was observed relative to the parent SBA-15 due to the increased thickness of the pore wall, demonstrating the organic functional groups and rhodium complex were grafted predominantly onto the internal surface of the pore. The HR-TEM images in Fig. S3 clearly demonstrate the mesoporous channels were preserved upon functionalization and immobilization of Wilkinson's complex and no metallic Rh nanoparticles were formed.

In order to further characterize differences in SBA-15 before and after functionalization and immobilization, we conducted ^{13}C and ^{29}Si solid-state NMR experiments. Fig. 1 shows the ^{29}Si CP-MAS NMR spectra for pure SBA-15, N-SBA-15, 2N-SBA-15, and P-SBA-15, respectively. As shown in Fig. 1A, two signals around −101 and −110 ppm for the pure SBA-15, characteristic of Q^3 and Q^4 silicon sites of the SiO_4-substructures ($Q^n = Si(OSi)_n(OH)_{4-n}$, n = 2–4) are present. The structural changes of the silica after the functionalization are visible in Fig. 1B, C, and D (spectra a, c, e). An additional set of peaks between −50 and −70 ppm, assignable to T^m-site groups ($T^m = RSi(OSi)_m(OH)_{3-m}$, m = 1–3) are present, indicating successful incorporation of organic moieties into the silica framework. An additional peak at -16 ppm assignable to —Si—O—$SiMe_3$ functionalities on P-SBA15 was observed for samples passivated with chlorotrimethylsilane prior to reaction with $LiPPh_2$. The subsequent immobilization of $RhCl(PPh_3)_3$ on the surface-functionalized SBA-15 causes marginal changes in the ^{29}Si CP-MAS spectra for the T^m and Q^n groups, as shown in Fig. 1B, C, and D (spectra b, d, f). It is unclear why T-groups for the P-SBA-15 and Rh-P-SBA-15 (Fig. 1) are so weak, but all other characterizations and reactivity studies are consistent with RhCl $(PPh_3)_3$ grafted to phosphine.

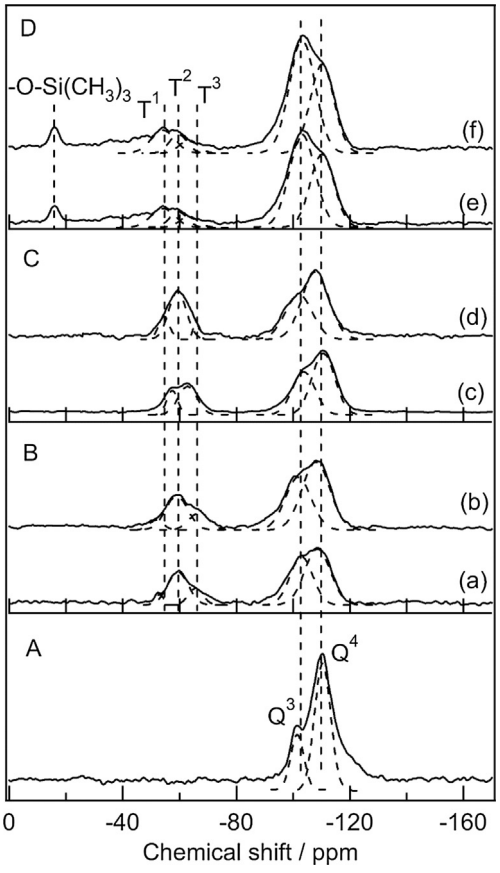

Fig. 1. ^{29}Si CP-MAS NMR spectra for (A) SBA-15; (B) a: N-SBA-15, b: Rh-N-SBA-15; (C) c: 2N-SBA-15, d: Rh-2N-SBA-15; (D) e: P-SBA-15 passivated with $ClSiMe_3$, f: Rh-P-SBA-15 passivated with $ClSiMe_3$.

Fig. 2 summarizes the ^{13}C CP-MAS NMR spectra for the SBA-15 upon organic functionalization and the corresponding catalysts after subsequent immobilization of $RhCl(PPh_3)_3$. Peaks corresponding to the pure organic functional linkers (Fig. 2A, spectrum a, 2B, d; and 2C, g) appear in the ^{13}C solid-state NMR spectra of the organically functionalized SBA-15 samples and their respective immobilized Rh complexes, indicating the successful grafting and structural retention of the organic linkers on the silica surface. Using N-SBA-15 as an example, the appearance of peaks at δ = 10.8, 18.6, 27.9, 45.4, and 58.6 ppm, corresponding to —$SiCH_2$, —OCH_2CH_3, —CH_2CHCH_2, —CH_2NH_2, and —OCH_2CH_3, respectively, demonstrates the successful grafting of 3-aminopropyl linkers to the SBA-15 surface through the condensation reaction between —OH and —$SiOCH_2CH_3$ (Fig. 2A, spectrum b). After subsequent immobilization of $RhCl(PPh_3)_3$, no significant differences in the ^{13}C CP-MAS NMR spectra were found among the catalysts with the exception of the appearance of a broad peak around δ = 128–132 ppm, assignable to the phenyl group of triphenylphosphine ligands coordinated to rhodium.

Notably, in the case of Rh-P-SBA-15 (Fig. 2C, spectrum k), the signal intensity of the phenyl group ranging from 128 to 132 ppm significantly increases; while the same signal for Rh-2N-SBA-15 (Fig. 2B, spectrum f) is virtually absent in the ^{13}C CP-MAS spectra. The most likely reason for this observation is due to the complete replacement of the PPh_3 ligand with the secondary-amine groups on the silica surface. Collectively, these results demonstrate the organic functional linkers and $RhCl(PPh_3)_3$ were successfully immobilized onto the surface of SBA-15. The results thus far demonstrate differences among grafted samples, but do not provide significant insight into the local structures of the individual immobilized Rh centers.

2.2. Local structure of the immobilized Rh complex on SBA-15

Various attempts towards the covalent immobilization of Wilkinson's complex, $RhCl(PPh_3)_3$, on a variety of solid supports have been undertaken and the resulting catalysts demonstrate high activity and stability during catalysis [27–34], but insufficient attention has been paid to the structure of the heterogenized catalyst. We deem this a critical element in the synthesis of supported molecular catalysts because knowledge of the local structure allows for the elucidation of structure-function relationships between activity/selectivity and the structure of the Rh center. To address this shortcoming, we applied a series of techniques in concert to obtain a better understanding of the chemical environment of surface-supported Rh complexes including ^{31}P CP-MAS NMR, 2D $^{31}P\{^1H\}$ HETCOR NMR, XPS, and Rh *K*-edge EXAFS.

2.2.1. Solid-State ^{31}P NMR characterization of immobilized Rh catalysts

Fig. 3 shows the ^{31}P CP-MAS NMR spectra for the as-prepared catalysts, Rh-N-SBA-15, Rh-2N-SBA-15, and Rh-P-SBA-15, respectively. The spectrum of Wilkinson's complex upon immobilization on the surface-functionalized SBA-15 differs significantly from the

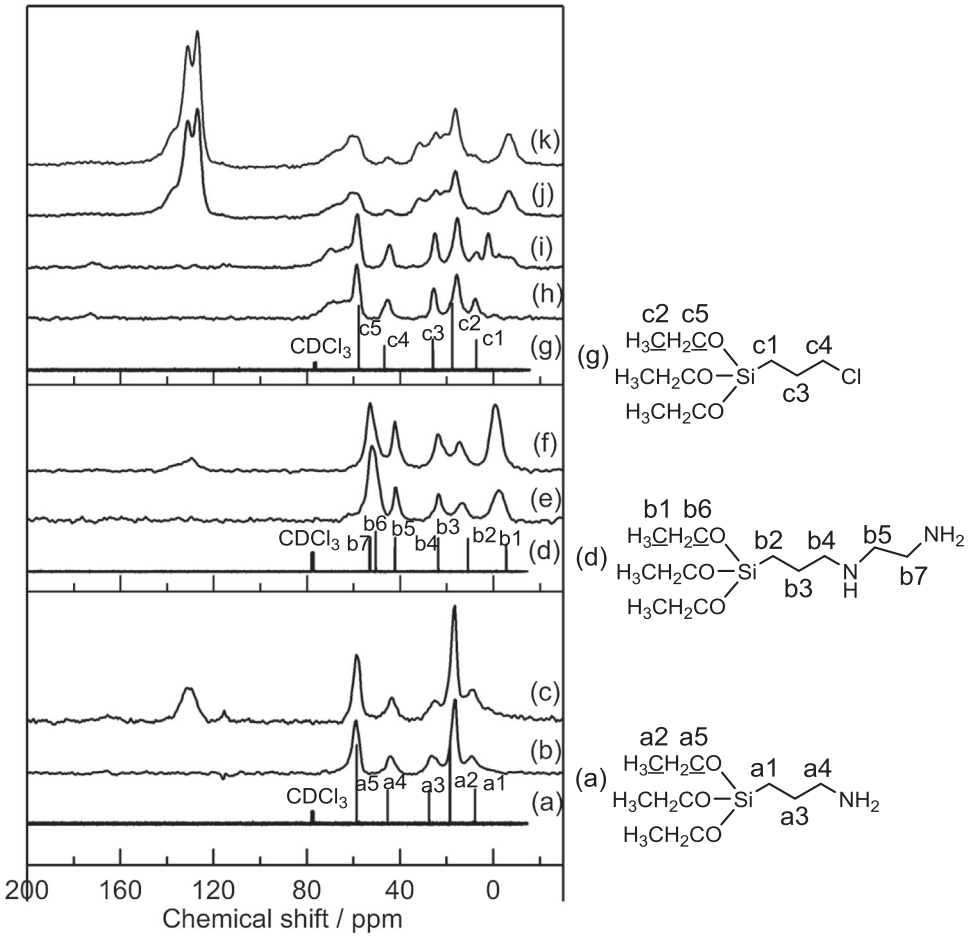

Fig. 2. ^{13}C liquid and CP-MAS NMR spectra for (a): (3-aminopropyl)triethoxysilane; (b): N-SBA-15, (c): Rh-N-SBA-15; (d): [3-(2-aminoethylamino)-propyl]triethoxysilane; (e): 2N-SBA-15, (f): Rh-2N-SBA-15; (g): 3-chloropropyltriethoxysilane, (h): Cl-SBA-15, (i): Cl-SBA-15 upon passivation with $ClSiMe_3$, (g): P-SBA-15, (k): Rh-P-SBA-15.

solid-state complex. The spectrum of the solid-state complex shows three center-split peaks with isotropic chemical shifts of 48.0, 32.5, and 22.3 ppm, attributable to the three nonequivalent phosphorus atoms in the complex molecule (Fig. 3A). Note that, in the solid state, $RhCl(PPh_3)_3$ has a distorted square planar structure in which the three phosphorous atoms are nonequivalent, the ^{31}P NMR spectrum therefore gives rise to the ABM part of an ABMX spectrum. The AB part of the spectrum is due to the two mutually trans ^{31}P nuclei, since $^2J(P,P)_{trans}$ couplings are usually found to be much larger than $^2J(P,P)_{cis}$. Analysis of the 1D CP/MAS spectrum of $RhCl(PPh_3)_3$ yields the following parameters: $\delta(P_1)$ = 22.3 ppm, $\delta(P_2)$ = 32.5 ppm, $\delta(P_3)$ = 48.0 ppm, $J_{(Rh\text{-}P1)}$ = 144 Hz, $J_{(Rh\text{-}P2)}$ = 140 Hz, and $J_{(Rh\text{-}P3)}$ = 194 Hz. Such results are in line with reported results [49]. A single broad symmetric peak at δ = 32.0 ppm was observed upon immobilization of $RhCl(PPh_3)_3$ onto N-SBA-15 (Fig. 3B, spectrum d), which is in good agreement with previously reported results [36]. After immobilization of $RhCl(PPh_3)_3$ onto 2N-SBA-15 (Fig. 3B, spectrum c), a single broad peak centered at δ = 28.6 ppm was detected albeit with a considerably lower intensity, compared with the other two immobilized Rh complexes, indicating a reduced number of triphenylphosphine groups are ligated to rhodium on the SBA-15 surface. This is in good agreement with previously discussed ^{13}C CP-MAS NMR and XPS results to be discussed in Section 2.2.3. Notably, a peak at δ = 0 ppm was observed, most likely due to the lower signal-to-noise ratio (even with long accumulation times common to solid state NMR) rather than deriving from a true P or Rh-P species on the surface of Rh-2N-SBA-15, which was further supported by XPS in Section 2.2.3.

In sharp contrast, two well-resolved peaks centered at δ = 27.0 and 44.0 ppm were observed upon immobilization of $RhCl(PPh_3)_3$ onto P-SBA-15 (Fig. 3B, spectrum b), indicative of two nonequivalent phosphorus groups coordinated to rhodium. Additionally, free grafted diphenylphosphine ligand at δ = −15.8 ppm was also observed. This peak position is in good agreement with the spectrum of P-SBA-15 (Fig. 3B, spectrum a). There is no indication of an oxidized phosphine peak (δ = 38.0 ppm) or phosphonium species (δ = 24.0 ppm) among the as-prepared catalysts [50,51], which is further supported by the XPS observation of P 2p binding energy (to be discussed in Section 2.2.3). An additional passivation step was performed to the P-SBA-15 material in order to eliminate the potential reaction between the basic $LiPPh_2$ and the remaining surface OH groups after grafting 3-chloropropyltriethoxysilane; the support surface was passivated by treatment with chlorotrimethylsilane to replace surface OH groups with $OSiMe_3$ groups. The removal of residual hydroxyl groups by passivation ensured a high probability of reaction between grafted propylchloride and $LiPPh_2$. We examined the necessity of this passivation step with solid-state ^{31}P NMR (Fig. S4). The ^{31}P spectra demonstrate very little difference between passivated and non-passivated P-SBA15 suggesting the reaction between $LiPPh_2$ was minor. As a consequence, the ^{31}P CP-MAS NMR results strongly indicate $RhCl(PPh_3)_3$ was successfully immobilized onto surface-functionalized

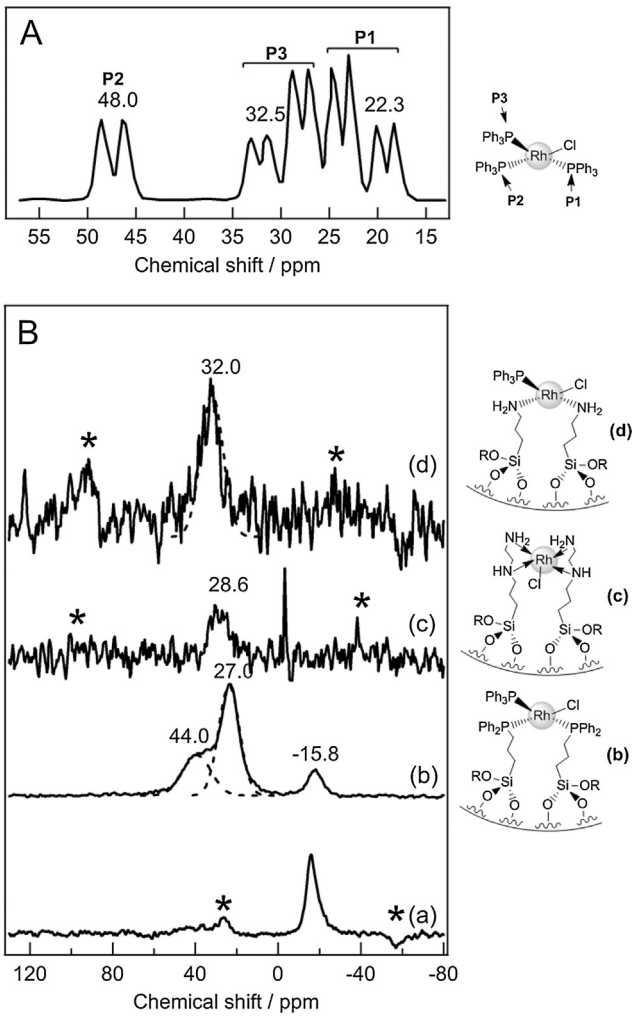

Fig. 3. ^{31}P CP-MAS NMR spectra for (A) RhCl(PPh$_3$)$_3$; (B) a: P-SBA-15, b: Rh-P-SBA-15, c: Rh-2N-SBA-15, d: Rh-N-SBA-15. Possible local structure of supported Rh complex is depicted next to the figure. Note: * represents spinning side bands.

SBA-15 with distinct differences in the exact structures of the local Rh complexes.

Supplementary data associated with this article can be found, in the online version, at https://doi.org/10.1016/j.jcat.2018.06.012.

2.2.2. 2D ^{31}P{^{1}H} HETCOR NMR characterization of immobilized Rh catalysts

The substantial breadth of the 1D ^{31}P CP-MAS NMR spectra prevents an accurate determination of the Rh-P coupling constants and determination of the non-equivalency of phosphorus atoms. Two-dimensional ^{31}P{^{1}H} HETCOR NMR experiments were conducted to provide additional information on the phosphorus species grafted to the surface of SBA-15 in order to gain insight into the local structure of the Rh site. The 2D spectra for the as-prepared catalysts Rh-P-SBA-15, Rh-N-SBA-15, and Rh-2N-SBA-15 are shown in Fig. 4A–C, respectively. The ^{31}P NMR peak at δ = −15.8 ppm from the grafted diphenylphosphine ligands on Rh-P-SBA-15 is strongly correlated to the methylene species (^{1}H NMR peaks ranging from 0.8 to 2.8 ppm) and to the aromatic rings (^{1}H NMR peaks, 7.0–7.5 ppm), as shown in Fig. 4A. An identical correlation was found for the ^{31}P NMR peak centered at δ = 27.0 ppm with the ^{1}H peaks at 0.8–2.8 and 7.0–7.5 ppm, suggesting 1 or 2 PPh$_3$ ligands are displaced when RhCl(PPh$_3$)$_3$ is grafted to P-SBA-15. The ^{31}P NMR peak centered at 44.0 ppm shows no correlation to the ^{1}H NMR peaks ranging from 0.8 to 2.8 ppm, but does show a correlation to the aromatic protons (^{1}H peaks, 7.0–7.5 ppm), which is attributed to the remaining PPh$_3$ ligated to rhodium. Deconvolution of the ^{31}P CP-MAS spectrum (Fig. 3, spectrum b) revealed the intensity ratio of peaks at δ = 27.0 and 44.0 ppm is ~2:1, indicating two equivalents of the tethered diphenylphosphine replaced two PPh$_3$ ligands to coordinate with rhodium upon immobilization of RhCl(PPh$_3$)$_3$ on the surface of SBA-15. The excess grafted diphenylphosphine increased the probability that adjacent free diphenylphosphine groups were available to ligate the same Rh center. For Rh-N-SBA-15, the ^{31}P NMR peak at 32 ppm, as expected, only has one correlation to the ^{1}H peak of the aromatic rings, as shown in Fig. 4B. However, a considerably weaker correlation between the ^{31}P and ^{1}H peaks was found in the case of Rh-2N-SBA-15, in accordance with the results of the 1D ^{31}P CP-MAS NMR experiment, further confirming the existence of trace phosphorus groups. The trace phosphorus species are most likely in the form of physically adsorbed RhCl(PPh$_3$)$_3$ on the surface even after thorough washing by Soxhlet extraction.

2.2.3. XPS characterization of immobilized Rh catalysts

Fig. S6 shows the XPS spectra for RhCl(PPh$_3$)$_3$, Rh-N-SBA-15, Rh-2N-SBA-15, and Rh-P-SBA-15, respectively. The binding energy (BE) value of Rh 3d$_{5/2}$ in RhCl(PPh$_3$)$_3$ was observed at 309.2 eV, in agreement with literature [52]. Upon immobilization of RhCl(PPh$_3$)$_3$ on the surface-functionalized SBA-15, the BE values of Rh 3d$_{5/2}$ differed from the homogeneous precursor. The magnitude of each BE shift relative to pure RhCl(PPh$_3$)$_3$ depended on the functional groups tethered to the SBA-15 surface as shown in Fig. S7. In the case of Rh-P-SBA-15, no distinct deviations in Rh 3d$_{5/2}$ BEs were observed. This result is reasonable because the electronic and steric characteristics of the immobilized rhodium complex was intrinsically retained upon immobilization since two PPh$_3$ ligands were replaced with two equivalent surface-tethered diphenylphosphines, as observed from 2D ^{31}P{^{1}H} HETCOR NMR. However, a significant shift to lower values in the BE of the Rh 3d$_{5/2}$ peak (307.9 and 307.5 eV) was found in Rh-N-SBA-15 and Rh-2N-SBA-15, respectively, and the shift in the case of Rh-2N-SBA-15 is slightly larger than Rh-N-SBA-15. We attribute the larger shift in Rh-2N-SBA-15 to twice as many amine interactions between the secondary-amine ligands, compared to the primary-amine, and rhodium. Primary and secondary amine ligands can replace two or even three PPh$_3$ ligands to coordinate with Rh during the formation of the immobilized Rh complexes because surface amine groups are stronger σ-electron donors than PPh$_3$ ligands. PPh$_3$ is a stronger π-acid than the amine ligands and the d-π back-donation decreases with the replacement of PPh$_3$ by —NH$_2$, thereby shifting the BEs of the Rh 3d$_{5/2}$ peaks to lower values [53]. Notably, no shift in the BE values of P 2p to 133.4 eV (phosphine oxide) [53] or 132.6 eV (phosphinium salt) [54] was observed, ruling out their on the immobilized Rh catalysts.

Table 1 summarizes the elemental composition for each catalyst measured by XPS. The observed results for the atomic ratio of P-to-Rh and Cl-to-Rh for RhCl(PPh$_3$)$_3$ matched the expected results of three and unity, respectively, while the atomic ratio of P-to-Rh varied among Rh-P-SBA-15, Rh-N-SBA-15, and Rh-2N-SBA-15. For Rh-N-SBA-15, the atomic ratio decreased to unity, suggesting only one PPh$_3$ remains ligated to rhodium. No significant phosphorus signal was detected for Rh-2N-SBA-15, suggesting near complete replacement of PPh$_3$ with surface-tethered secondary amine groups on the surface of SBA-15. The lack of phosphorous signal is likely due to the lower sensitivity of XPS compared to ^{31}P CP-MAS NMR. In the case of Rh-P-SBA-15, owing to an excess of free tethered diphenylphosphine ligands on the SBA-15 surface, the atomic ratio of P-to-Rh exceeds three. Such a

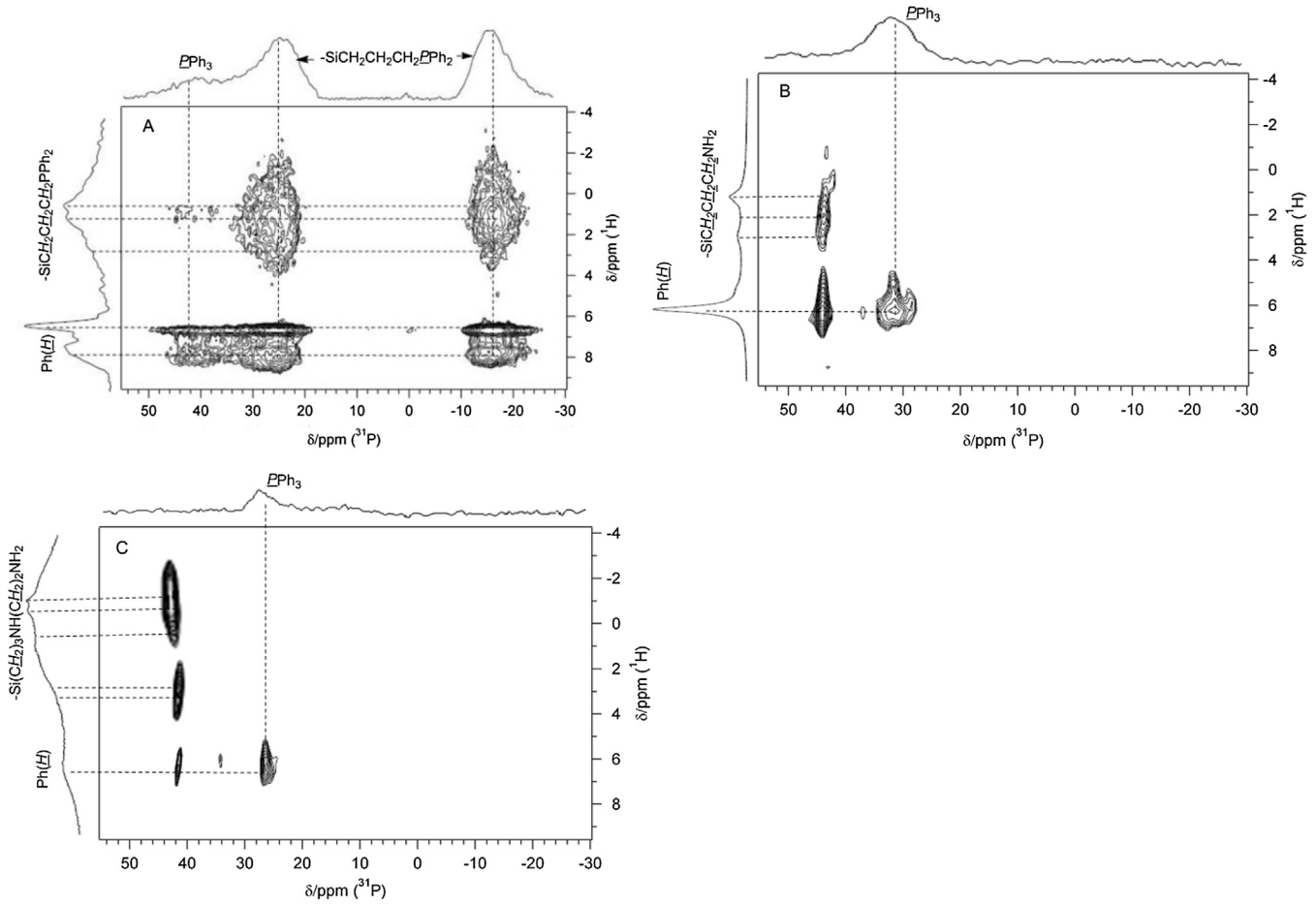

Fig. 4. ^{31}P {^{1}H} HETCOR (heteronuclear correlation) NMR for (A) Rh-P-SBA-15; (B) Rh-N-SBA-15; (C) Rh-2N-SBA-15.

Table 1
Elemental composition measured by XPS for $RhCl(PPh_3)_3$ and the Rh-grafted catalysts.

Sample	Binding Energy (eV)				Relative Concentration (atom %)				P/Rh	Cl/Rh
	N (1s)	P (2p)	Cl (2p)	Rh ($3d_{3/2}/3d_{5/2}$)	N	P	Cl	Rh		
$RhCl(PPh_3)_3$	–	132.1	198.1	314.3/309.2	–	4.90	1.54	1.65	2.97	0.93
Rh-N-SBA-15	399.6	131.6	198.2	312.8/307.9	3.93	0.68	0.84	0.65	1.05	1.29
Rh-2N-SBA-15	399.1	–	198.1	312.3/307.5	6.60	–	1.06	1.09	–	0.97
Rh-P-SBA-15	–	132.1	198.0	314.4/309.2	–	2.52	0.77	0.72	3.50	1.07

value is reasonable and agrees with ^{31}P NMR results (Fig. 3, spectrum b). The atomic ratio of Cl-to-Rh (1:1) in each as-prepared catalyst is constant at the stoichiometry of the neat complex, demonstrating Cl is not replaced during immobilization.

2.2.4. EXAFS characterization of immobilized Rh catalysts

Rh *K*-edge EXAFS experiments were conducted to further characterize the local structure of the immobilized Rh complexes. Fig. 5 is a compilation of the collected spectra and Table 2 summarizes the fitting results. In Fig. 5, the solid lines represent the experimental data while the dashed lines represent the phase-corrected fitted models. For Rh-P-SBA-15, the coordination number, *N*, was found to be 2.00 and 2.00 for Rh-P and Rh-Cl, respectively (experimental details are provided in Section 4.8 of the Supporting Information). Due to the similar interatomic distance and electronic structure of Rh-Cl and Rh-P, distinguishing between P and Cl atoms is difficult. Considering that the Cl:Rh ratio was determined to be unity for Rh-P-SBA-15 from XPS, we interpret our EXAFS results as confirmation that three phosphine-containing ligands are grafted to the Rh center. ^{31}P NMR results (both 1D and 2D) allows us to differentiate between these phosphine-containing ligands as a single PPh_3 ligand and a pair of diphenylphosphine ligands. For the immobilized Rh-2N-SBA-15 catalyst, we excluded a Rh-P scattering path for our EXAFS fitting due to the lack of P signals from both the XPS and NMR results. The fitting for Rh-2N-SBA-15 shows *N* values of 4.05 and 0.95 for Rh-N and Rh-Cl, respectively. These results also support the proposed structure with the local atomic environments consisting of 4 Rh-N bonds and 1 Rh-Cl bond. Finally, for Rh-N-SBA-15, the *N* values were found to be 0.80, 1.09, and 2.11 for Rh-P, Rh-Cl, and Rh-N, respectively. The ratio of these numbers is close to the proposed structure (1:1:2 for P:Cl:N). No Rh-Rh scattering path could be fit in any of the samples, thereby ruling out the formation of metallic Rh nanoparticles. This result is in good agreement with HR-TEM observation and results of Hg(0) poisoning experiments as shown in Scheme S1. Overall, our EXAFS results show that the local atomic structures agree with the proposed

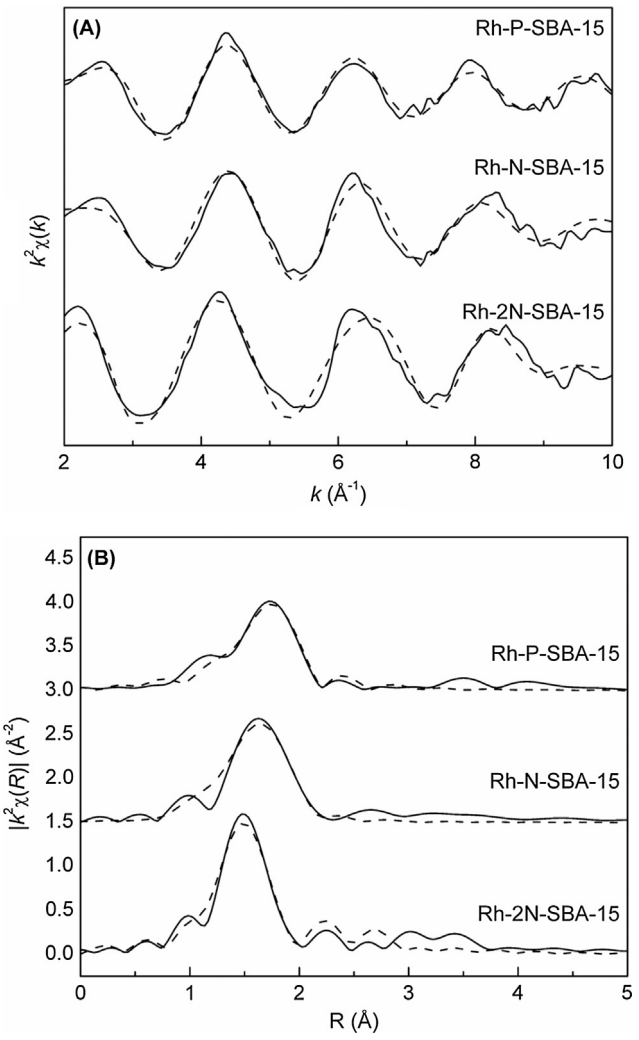

Fig. 5. (A) k^2-weighted and (B) Fourier transform of Rh *K*-edge EXAFS spectra of the supported Rh catalysts.

structures from our XPS and NMR results, including retention of the Cl ligand upon immobilization among all types of grafted organic functional groups. Based on the above characterization results, the local structure of the immobilized Rh-complexes upon reaction of $RhCl(PPh_3)_3$ with functionalized SBA-15 bearing primary amine, or secondary amine, or diphenylphosphine groups are proposed in Fig. 3.

2.3. Catalytic performance of grafted Rh-(N, 2N, P)-SBA-15 catalysts

2.3.1. Catalytic hydrothiolation of alkynes with thiols

Several metal-based homogeneous catalysts such as Rh [55–60], Ir [61], Ni [62,63], Cu [64,65], Pd [66,67], Pt [68], Au [69], Zr [70–72], and f-elements [70–72] have been developed to produce regio- and stereoselective vinyl sulfides, which are versatile intermediates for the synthesis of biologically active compounds, organic building blocks, and new materials. However, highly regio- and stereoselective hydrothiolation of a wide range of alkynes with various thiols catalyzed by a heterogeneous catalyst is still not readily available to date. Given the utility and proficiency of homogeneous Rh complexes for alkyne hydrothiolation as previously reported [55–60], we developed immobilized Rh complex catalysts with different grafting ligands for the hydrothiolation of alkynes with thiols (see Table S2 for hydrothiolation reaction data) [39]. The homogeneous Wilkinson's complex, $RhCl(PPh_3)_3$, showed high activity and excellent regio- and stereoselectivity for the addition of phenylacetylene (**1a**) to thiophenol (**1b**), achieving up to 98% conversion and 94% selectivity to *E*-**1ab** along with 6% selectivity to the Markovnikov adduct in DCE at room temperature within 45 min, as shown in Scheme 2. The immobilized Rh complexes – Rh-N-SBA-15, Rh-2N-SBA-15, and Rh-P-SBA-15 – exhibited similar conversions (around 80%) after 20 h. The stereoselectivity differed depending on the functional groups linked to the Rh complex, though all immobilized catalysts were completely regioselective to the *anti*-Markovnikov product. The Rh-N-SBA-15 catalyst gave a mixture of *anti*-Markovnikov ((*E* + *Z*)-**(1 + 2)ab**) products with the (*Z*)-isomer (**1ab**) as the main product, while Rh-2N-SBA-15 produced *Z*-**2ab** with 99% stereoselectivity. In sharp contrast, exclusive and reversed stereoselectivity to *E*-**1ab** was obtained in the presence of Rh-P-SBA-15 under otherwise identical reaction conditions. The Markovnikov addition was completely suppressed upon immobilization of $RhCl(PPh_3)_3$ onto surface-functionalized SBA-15.

In order to better understand the relationship between the local structure and catalytic hdyrothiolation activity/selectivity of the immobilized catalysts, two equivalents of organic amine with respect to $RhCl(PPh_3)_3$ were mixed with phenylacetylene and thiophenol in solution. A dramatic decrease in catalytic activity with significant change in stereoselectivity was observed compared to the reaction without the addition of amine in the presence of $RhCl(PPh_3)_3$. A conversion of 92.0% with 30/70 of *E*/*Z* stereoselectivity to **2ab** was observed after 20 h at room temperature (Scheme 3) when 2 equivalent of propylamine was added. This result is roughly equal to the activity and stereoselectivity of the Rh-N-SBA-15 catalyst. Likewise, excellent stereoselectivity to *Z*-**2ab** (96%) at lower conversion (61.2%) comparable to the Rh-2N-SBA-15 catalyst was afforded when 2 equivalents of *N*--

Table 2
Curve-fitting analysis for the Rh *K*-edge EXAFS data.[a]

Sample	Path	N[b]	R(Å)[c]	ΔE_0(eV)[d]	$1000 \times \sigma^{2}$[e](Å^2)
Rh-P-SBA-15	Rh-P	3.04 ± 0.6	2.29 ± 0.02	−3.6 ± 4.4	5 ± 1
	Rh-Cl	0.96 ± 0.6	2.37 ± 0.02	−1.2 ± 1.2	5 ± 1
Rh-N-SBA-15	Rh-P	0.80 ± 0.2	2.29 ± 0.02	−2.0 ± 0.8	3 ± 1
	Rh-N	1.09 ± 0.3	2.08 ± 0.02	0.9 ± 1.8	3 ± 1
	Rh-Cl	2.11 ± 0.3	2.37 ± 0.02	−5.3 ± 1.7	3 ± 1
Rh-2N-SBA-15	Rh-N	4.05 ± 0.5	2.08 ± 0.02	−9.7 ± 2.1	3 ± 1
	Rh-Cl	0.95 ± 0.1	2.37 ± 0.02	7.5 ± 2.6	3 ± 1

[a] Fourier transform and inverse Fourier transform regions were limited, where Δk = 2–10.0 Å^{-1} and Δr = 1.0–3.0 Å, respectively. Curve-fitting analysis was performed for the Rh K-edge.
[b] Coordination number.
[c] Bond distance between absorber and backscatter atoms.
[d] The inner potential correction accounts for the difference in the inner potential between the sample and reference.
[e] The Debye-Waller factor (σ^2), is a measure of the thermal disorder in the system assumed identical for every path in a sample.

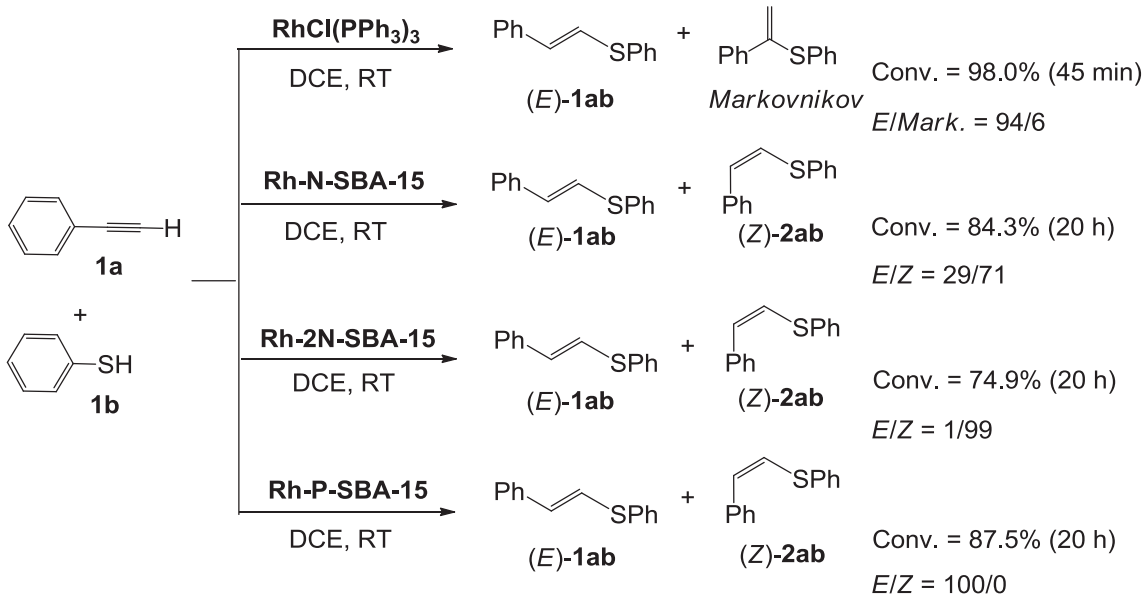

Scheme 2. Product distribution for the hydrothiolation of phenylacetylene and thiophenol over different Rh catalysts. Reaction conditions: 0.5 mmol phenylacetylene, 0.55 mmol thiophenol, 50 mg catalyst (4.5 μmol Rh), 2 mL DCE and room temperature.

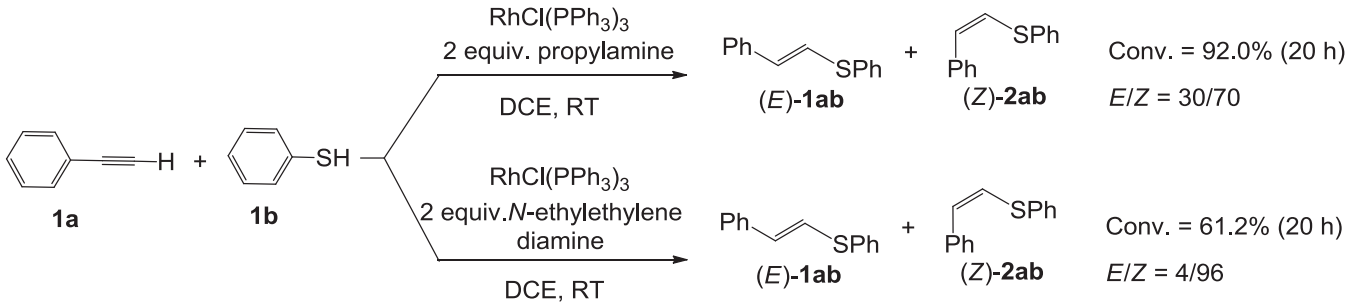

Scheme 3. Product distribution for the hydrothiolation of phenylacetylene and thiophenol over $RhCl(PPh_3)_3$ with 2 equivalents of propylamine or *N*-ethylethylenediamine. Reaction conditions: 4.5 μmol $RhCl(PPh_3)_3$, 0.5 mmol phenylacetylene, 0.55 mmol thiophenol, 2 mL DCE, and room temperature.

ethylethylenediamine were introduced into the reaction under otherwise identical reaction conditions (Scheme 3). These findings demonstrate the amino functional groups (either primary or secondary) significantly influence the activity and stereoselectivity of alkyne hydrothiolation catalyzed by $RhCl(PPh_3)_3$ by displacing amino groups with PPh_3 ligand of $RhCl(PPh_3)_3$, which was further evidenced by liquid ^{31}P NMR characterization as presented in Fig. S5. After Wilkinson's complex $RhCl(PPh_3)_3$ reacted with 2 equivalents of propylamine (relative to $RhCl(PPh_3)_3$) in DCE at room temperature for 2 h, the signal for the characteristic ^{31}P NMR peaks of $RhCl(PPh_3)_3$ in DCE decreased, and free PPh_3 was observed due to the exchange reaction between propylamine and PPh_3 ligands with concomitant formation of a new Rh species at δ = 27.8 ppm. After reaction with 2 equivalents of *N*-ethylethylenediamine, the characteristic ^{31}P NMR peaks for $RhCl(PPh_3)_3$ disappeared with near complete release of PPh_3 (δ = −5.0 ppm) in DCE. These results are consistent with ^{31}P solid state NMR results for Rh-N-SBA-15 and Rh-2N-SBA-15. We have not identified the products of ligand exchange, but the combined catalytic results and ^{31}P NMR characterization of ligand exchange are consistent with amine displacing phosphine from the Rh center. Such outcomes obtained from the control experiments verify the chemistry of the replacement of grafted amino functional groups with PPh_3 ligand upon immobilization of $RhCl(PPh_3)_3$ and further confirm the relationship between the catalytic activity/selectivity with the structure of the immobilized Rh center.

Mechanistic investigations point to a catalytic cycle initiated by oxidative addition of the thiol with Rh center to generate a hydride thiolate (H-Rh-SR) species and subsequent alkyne insertion into the hydride ligand followed by reductive elimination to afford the *anti*-Markovnikov (*E*, *Z*, or both) adducts [60,73]. The formation of *Z*-β-vinyl sulfides generally requires isomerization of metal alkenyl intermediates prior to reductive elimination [74,75]. It appears the active Rh species coordinated to amino-groups preferentially favors the isomerization to produce *Z*-β-vinyl sulfides based on our findings over both homogeneous and heterogeneous N-ligated Rh centers.

2.3.2. Catalytic hydrosulfonation of alkynes with sulfonic acids over immobilized Rh catalysts

The most straightforward and atom-economical method to access vinyl sulfonates is via transition-metal catalyzed regioselective intermolecular addition of sulfonic acids to alkynes. Although transition-metal-catalyzed addition of alkynes to various nucleophilic reagents such as water [76–80], alcohols [81–87], amines [61,88–97], thiols [38,58,60,68,70–73,98,99], carboxylic acids [100–103], and sulfonic acids [104] for the formation of regio- and stereo-defined vinyl C-heteroatom products have been

developed, only a few catalytic systems have been reported for the regioselective addition of sulfonic acids to alkynes [105–107]. Previous approaches to synthesize vinyl sulfonates suffered from complicated synthesis of starting materials, tedious work-up procedures, low regioselectivity, and limited substrate versatility [108–111]. Studies documenting regio- and stereoselective additions over supported metal catalysts are not available thus far, to the best of our knowledge. Therefore, development of a stable heterogeneous catalyst that allows for highly regio- and stereoselective addition of alkynes to sulfonic acids to form the corresponding vinyl sulfonates is of great interest.

As discussed above, the regio- and stereoselectivity to the desired vinyl sulfides for hydrothiolation of alkynes with thiols is controlled by the local structure of the immobilized Rh complexes. We tested the ability of Wilkinson's catalyst to perform hydrosulfonation reactions using 1.0 mol % catalyst in 2 mL DCE at 70 °C in the presence of 1.0 mmol phenylacetylene and 0.5 mmol methanesulfonic acid. We achieved 86.2% yield (based on conversion of methanesulfonic acid) to the Markovnikov product after 2 h. We then performed the addition of phenylacetylene with methanesulfonic acid to form vinyl sulfonates catalyzed by Rh-P-SBA-15, Rh-N-SBA-15, and Rh-2N-SBA-15, respectively, in DCE at 70 °C. The immobilized catalysts displayed comparable activity and absolute regioselectivity to Markovnikov vinyl sulfonates, as shown in Scheme S2. The regioselectivity is independent of the local structure of the immobilized Rh complexes, which is completely different and opposite to the *anti*-Markovnikov adducts formed during hydrothiolation. We screened a limited number of alkyne and sulfonic acid substrates over Rh-P-SBA-15 and the results are summarized in Table 3. Alkynes were hydrosulfonated with methanesulfonic acid to produce the corresponding Markovnikov vinyl sulfonates in moderate to high conversion with absolute regioselectivity. A group of phenylacetylenes bearing electron-rich (**5**-**8a**) and electron-poor substituents (**10**, **11a**) at *o*-, *m*-, or *p*- positions on the phenyl ring reacted efficiently with methanesulfonic acid. The electron-poor substituents exhibited a negative effect on the reaction, resulting in considerably lower conversions under otherwise identical reaction conditions. Internal alkynes underwent regioselective hydrosulfonation to afford the corresponding Markovnikov adducts (**20**, **21ab**) with satisfactory conversions, but required longer reaction times.

Aromatic sulfonic acids featuring both electron-donating (**16**, **17b**) and electron-withdrawing groups (**18**, **19b**) could be added to phenylacetylene efficiently to afford the corresponding vinyl sulfonate esters in moderate to high conversions with exclusive regioselectivity. Stronger acids are beneficial for this transformation. The addition of 4-chlorobenzenesulfonic acid to phenylacetylene was converted into the corresponding vinyl sulfonate

Table 3
Scopes of alkynes and sulfonic acids for hydrosulfonation.[a]

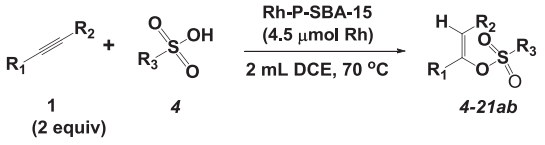

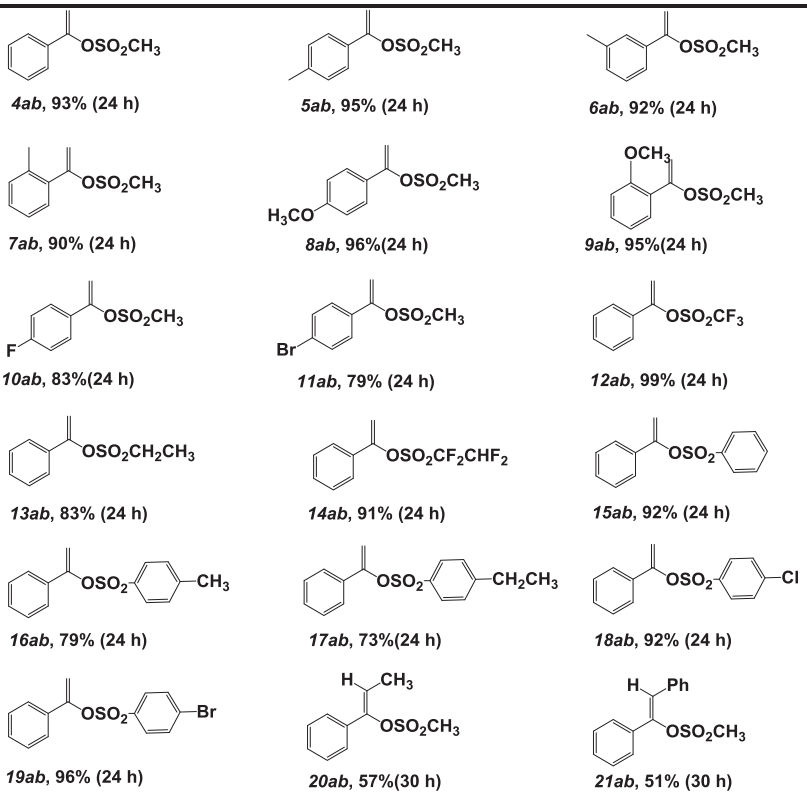

[a] Reaction conditions: 1 mmol alkyne, 0.50 mmol sulfonic acid, 50 mg catalyst Rh-P-SBA-15 (4.5 μmol Rh), 2 mL DCE and 70 °C. The reported yield is based on the quantity of isolated product.

(**18ab**) in 92.4% yield after 24 h, while 73.2% yield of **17ab** for the addition of 4-ethylbenzensulfonic acid with phenylacetylene was achieved under otherwise identical reaction conditions. Functional groups on the alkynes such as fluoro, chloro, hydroxyl, and methoxy were compatible with this catalytic system. In all cases listed in Table 3, no double bond isomerization occurred.

2.4. Stability and recyclability of the immobilized Rh catalysts during hydrosulfonation

In our previous studies, we found the immobilized Rh complexes to be stable for the hydrothiolation of alkynes with thiols [39]. We also examined the stability of the immobilized Rh complexes during hydrosulfonation reactions. First, to verify whether the observed catalysis was due to the heterogeneous catalyst, Rh-P-SBA-15, or a leached rhodium species in solution, we carried out the addition of phenylacetylene (**1a**) to methanesulfonic acid (**4b**) and removed the catalyst from the reaction mixture by hot-filtration at approximately 50% conversion of **4b** (Fig. S8) at 70 °C. After removal of Rh-P-SBA-15, the filtrate was again held at the same temperature under an atmosphere of N_2. No significant increase in conversion was observed, indicating leached Rh species from the catalyst are not responsible for the observed activity. ICP-AES analysis provided further confirmation that no rhodium species was detected in the filtrate (below detection limit). The Rh-P-SBA-15 catalyst was recovered and could be reused up to four times for the transformation of **1a** and **4b** without any significant loss of catalytic activity and regioselectivity, as shown in Fig. S9. Together, these results rule out any contribution to the observed catalysis from a homogeneous rhodium species, confirming the observed catalysis was intrinsically heterogeneous. Additionally, results for ^{31}P CP-MAS NMR of the grafted catalysts after reaction showed little change in the local structure of the grafted Rh-complexes (Fig. S10).

3. Conclusions

The structure of immobilized Rh complexes derived from the reaction of Wilkinson's complex $RhCl(PPh_3)_3$ with surface-functionalized SBA-15 bearing primary or secondary amine and diphenylphosphine functional groups within the mesoporous channels have been elucidated. Their structure strongly depended on the surface-tethered functional groups replacing two or three PPh_3 ligands of $RhCl(PPh_3)_3$ on SBA-15 during the transformation, which were systematically identified by a series of techniques including ^{31}P CP-MAS NMR, $^{31}P\{^1H\}$ HETCOR NMR, XPS, and Rh *K*-edge EXAFS. The resulting immobilized Rh complexes exhibited high activity for the addition of alkynes with thiols or sulfonic acids, respectively. The regio- and stereoselectivity for hydrothiolation to yield vinyl sulfides depended on the local structures of grafted Rh complexes and the stereoselectivity could be readily switched. In contrast, only Markovnikov vinyl sulfonate esters were produced for the addition of alkynes with sulfonic acids without such a dependence on the local structure of the grafted Rh complexes. A wide range of substrates (alkynes, thiols, and sulfonic acids) could be efficiently added to form their corresponding adducts. The immobilized Rh-complexes could be reused several times without significant loss in catalytic activity and regio- and stereoselectivity for hydrothiolation and hydrosulfonation. This study demonstrates that in order to understand why a particular catalyst is or is not active and selective; it is paramount to determine the local structure of the surface organometallic catalyst which ultimately requires complimentary spectroscopic techniques if both the inner ligand sphere and metal center are to be characterized.

Acknowledgements

Y. Y., J. W. C. and R.M.R. acknowledge funding from the Department of Energy, Office of Basic Energy Sciences, Chemical Sciences, Geosciences, and Biosciences Division, Catalysis Sciences Program under grant number DE-SC0016192. X-ray absorption measurements were made on the 10-BM-A beamline of the Materials Research Collaborative Access Team (MRCAT) at the Advanced Photon Source, Argonne National Laboratory (Argonne, IL). MRCAT operations are supported by the Department of Energy and the MRCAT member institutions. This research used resources of the Advanced Photon Source, a U.S. Department of Energy (DOE) Office of Science User Facility operated for the DOE Office of Science by Argonne National Laboratory under Contract No. DE-AC02-06CH11357. Y.Y acknowledge the start-up financial support from Qingdao Institute of Bioenergy and Bioprocess Technology (QIBEBT), Chinese Academy of Sciences (Grant No. Y6710619KL). We also thank Dr. Yu Noda and Dr. Eric Moschetta for additional solidstate NMR experiments.

References

[1] Y. Iwasawa, Tailored Metal Catalysts, D. Reidel Pub. Co., Dordrecht; Boston Hingham, MA, U.S.A., 1986.
[2] M. Dusi, T. Mallat, A. Baiker, Epoxidation of functionalized olefins over solid catalysts, Catal. Rev. - Sci. Eng. 42 (2000) 213–278.
[3] R.M. Rioux, Model Systems in Catalysis: Single Crystals to Supported Enzyme Mimics, Springer, New York, 2010.
[4] A.J. Sandee, J.N.H. Reek, P.C.J. Kamer, P.W.N.M. van Leeuwen, A silica-supported, switchable, and recyclable hydroformylation-hydrogenation catalyst, J. Am. Chem. Soc. 123 (2001) 8468–8476.
[5] C. Merckle, J. Blumel, Improved rhodium hydrogenation catalysts immobilized on oxidic supports, Adv. Synth. Catal. 345 (2003) 584–588.
[6] S.-G. Shyu, S.-W. Cheng, D.-L. Tzou, Immobilization of $Rh(PPh_3)_3Cl$ on phosphinated MCM-41 for catalytic hydrogenation of olefins, Chem. Commun. 2337–2338 (1999).
[7] Q. Peng, Y. Yang, Y. Yuan, Immobilization of rhodium complexes ligated with triphenyphosphine analogs on amino-functionalized MCM-41 and MCM-48 for 1-hexene hydroformylation, J. Mol. Catal. A: Chem. 219 (2004) 175–181.
[8] W. Zhou, D. He, A facile method for promoting activities of ordered mesoporous silica-anchored Rh-P complex catalysts in 1-octene hydroformylation, Green Chem. 11 (2009) 1146–1154.
[9] S.C. Bourque, F. Maltais, W.-J. Xiao, O. Tardif, H. Alper, P. Arya, L.E. Manzer, Hydroformylation reactions with rhodium-complexed dendrimers on silica, J. Am. Chem. Soc. 121 (1999) 3035–3038.
[10] F. Marras, J. Wang, M.-O. Coppens, J.N.H. Reek, Ordered mesoporous materials as solid supports for rhodium-diphosphine catalysts with remarkable hydroformylation activity, Chem. Commun. 46 (2010) 6587–6589.
[11] Y. Yang, R.M. Rioux, Highly stereoselective anti-Markovnikov hydrothiolation of alkynes and electron-deficient alkenes by a supported Cu-NHC complex, Green Chem. 16 (2014) 3916–3925.
[12] R. Sayah, E. Framery, V. Dufaud, Asymmetric hydrogenation using Wilkinson-type rhodium complexes immobilized onto mesoporous silica, Green Chem. 11 (2009) 1694–1702.
[13] B. Marciniec, K. Szubert, R. Fiedorow, I. Kownacki, M.J. Potrzebowski, M. Dutkiewicz, A. Franczyk, Catalysis of hydrosilylation by well-defined rhodium siloxide complexes immobilized on silica, J. Mol. Catal. A: Chem. 310 (2009) 9–16.
[14] M. Tada, R. Coquet, J. Yoshida, M. Kinoshita, Y. Iwasawa, Selective formation of a coordinatively unsaturated metal complex at a surface: a SiO_2-immobilized three-coordinate ruthenium catalyst for alkene epoxidation, Angew. Chem., Int. Ed. 46 (2007) 7220–7223.
[15] J.M. Thomas, R. Raja, D.W. Lewis, Single-site heterogeneous catalysts, Angew. Chem., Int. Ed. 44 (2005) 6456–6482.
[16] P. McMorn, G.J. Hutchings, Heterogeneous enantioselective catalysts: strategies for the immobilisation of homogeneous catalysts, Chem. Soc. Rev. 33 (2004) 108–122.
[17] C. Coperet, J.M. Basset, Strategies to immobilize well-defined olefin metathesis catalysts: supported homogeneous catalysis vs surface organometallic chemistry, Adv. Synth. Catal. 349 (2007) 78–92.
[18] C. Li, Chiral synthesis on catalysts immobilized in microporous and mesoporous materials, Catal. Rev. - Sci. Eng. 46 (2004) 419–492.
[19] T.J. Terry, T.D.P. Stack, Covalent heterogenization of a discrete Mn(II) bis-phen complex by a metal-template/metal-exchange method: an epoxidation catalyst with enhanced reactivity, J. Am. Chem. Soc. 130 (2008) 4945–4953.
[20] D. Evans, J.A. Osborn, G. Wilkinson, Hydroformylation of alkenes by use of rhodium complex catalysts, J. Chem. Soc. A 3133–3142 (1968).
[21] J.M. Brown, A.R.J. Lucy, Origins of enantioselectivity in catalytic asymmetric synthesis, Chem. Soc. Chem. Commun. (1984) 914–915.

[22] N. Kameda, R. Igarashi, Homogeneous catalytic hydrogenation of olefins using $RhH_2(Ph_2{}_N3)(PP_h3)2$ in tetrahydrofuran, J. Mol. Catal. 75 (1992) 15–20.
[23] X. Guo, P.J. Scott, G.L. Rempel, Catalytic hydrogenation of diene polymers: Part II. Kinetic analysis and mechanistic studies on the hydrogenation of styrene-butadiene copolymers in the presence of $RhCl(PPh_3)_3$, J. Mol. Catal. 72 (1992) 193–208.
[24] J.M. O'Connor, J. Ma, Metal-catalyzed decarbonylation of primary aldehydes at room temperature, J. Org. Chem. 57 (1992) 5075–5077.
[25] K. Ohno, J. Tsuji, Organic synthesis by means of noble metal compounds. XXXV. Novel decarbonylation reactions of aldehydes and acyl halides using rhodium complexes, J. Am. Chem. Soc. 90 (1968) 99–107.
[26] F.H. Jardine, Chlorotris(triphenylphosphine)rhodium(I): its chemical and catalytic reactions, Prog. Inorg. Chem. 28 (1981) 63–202.
[27] M.E. Quiroga, E.A. Cagnola, D.A. Liprandi, P.C. L'Argentiere, Supported Wilkinson's complex used as a high active hydrogenation catalyst, J. Mol. Catal. A: Chem. 149 (1999) 147–152.
[28] S. Banerjee, S.S. Wong, Structural characterization, optical properties, and improved solubility of carbon nanotubes functionalized with Wilkinson's catalyst, J. Am. Chem. Soc. 124 (2002) 8940–8948.
[29] C. Merckle, S. Haubrich, J. Blumel, Immobilized rhodium hydrogenation catalysts, J. Organomet. Chem. 627 (2001) 44–54.
[30] E. Arstad, A.G.M. Barrett, L. Tedeschi, ROMP gel-supported tris (triphenylphosphine)rhodium(I) chloride: a selective hydrogenation catalyst for parallel synthesis, Tetrahedron Lett. 44 (2003) 2703–2707.
[31] K. Bogar, P. Krumlinde, Z. Bacsik, N. Hedin, J.-E. Baeckvall, Heterogenized Wilkinson-type catalyst for transfer hydrogenation of carbonyl compounds, Eur. J. Org. Chem. 2011 (2011) 4409–4414.
[32] J. Kramer, E. Nollen, W. Buijs, W.L. Driessen, Reedijk, Investigations into the recovery of Wilkinson's catalyst with silica-immobilised P-donor ligands, J. React. Funct. Polym. 57 (2003) 1–11.
[33] S.K. Tanielyan, R.L. Augustine, N. Marin, G. Alvez, Anchored Wilkinson catalyst, ACS Catal. 1 (2011) 159–169.
[34] M. Perez-Cadenas, L.J. Lemus-Yegres, M.C. Roman-Martinez, d.L.C. Salinas-Martinez, Immobilization of a Rh complex derived from the Wilkinson's catalyst on activated carbon and carbon nanotubes, Appl. Catal., A 402 (2011) 132–138.
[35] C. Coperet, M. Chabanas, R.P. Saint-Arroman, J.-M. Basset, Homogeneous and heterogeneous catalysis: bridging the gap through surface organometallic chemistry, Angew. Chem., Int. Ed. 42 (2003) 156–181.
[36] A. Grunberg, X. Yeping, H. Breitzke, G. Buntkowsky, Solid-state NMR characterization of Wilkinson's catalyst immobilized in mesoporous SBA-3 silica, Chem. Eur. J. 16 (2010) 6993–6998.
[37] J.-R. Chang, H.-M. Lin, S.-W. Cheng, C.-K. Tseng, D.-L. Tzou, S.-G. Shyu, EXAFS investigation of the morphology of immobilized $Rh(PPh_3)_3Cl$ on phosphinated MCM-41, J. Mol. Catal. A: Chem. 329 (2010) 27–35.
[38] J. Blüemel, Linkers and catalysts immobilized on oxide supports: new insights by solid-state NMR spectroscopy, Coord. Chem. Rev. 252 (2008) 2410–2423.
[39] Y. Yang, R.M. Rioux, Highly regio- and stereoselective hydrothiolation of acetylenes with thiols catalyzed by a well-defined supported Rh complex, Chem. Commun. 47 (2011) 6557–6559.
[40] K. Ritter, Synthetic transformations of vinyl and aryl triflates, Synthesis (1993) 735–762.
[41] F. Diederich, P.J. Stang, Metal-Catalyzed Cross-Coupling Reactions, Wiley-VCH, New York, 1998.
[42] M.E. Limmert, A.H. Roy, J.F. Hartwig, Kumada coupling of aryl and vinyl tosylates under mild conditions, J. Org. Chem. 70 (2005) 9364–9370.
[43] W.J. Scott, G.T. Crisp, J.K. Stille, Palladium-catalyzed coupling of vinyl triflates with organostannanes. A short synthesis of pleraplysilin-1, J. Am. Chem. Soc. 106 (1984) 4630–4632.
[44] K.D. Hesp, R.J. Lundgren, M. Stradiotto, Palladium-catalyzed mono-α-arylation of acetone with aryl halides and tosylates, J. Am. Chem. Soc. 133 (2011) 5194–5197.
[45] D.C. Reeves, S. Rodriguez, H. Lee, N. Haddad, D. Krishnamurthy, C.H. Senanayake, Palladium catalyzed alkoxy- and aminocarbonylation of vinyl tosylates, Org. Lett. 13 (2011) 2495–2497.
[46] H. Mori, E. Kudo, Y. Saito, A. Onuma, M. Morishima, RAFT polymerization of vinyl sulfonate esters for the controlled synthesis of poly(lithium vinyl sulfonate) and sulfonated block copolymers, Macromolecules 43 (2010) 7021–7032.
[47] P.J. Stang, Vinyl triflate chemistry: unsaturated cations and carbenes, Acc. Chem. Res. 11 (1978) 107–114.
[48] D.-Y. Zhao, J.-L. Feng, Q.-S. Huo, N. Melosh, G.H. Fredrickson, B.F. Chmelka, G. D. Stucky, Triblock copolymer synthesis of mesoporous silica with periodic 50 to 300 angstrom pores, Science 279 (1998) 548–552.
[49] G. Wu, R.E. Wasylishen, Applications of two-dimensional phosphorus-31 CP/MAS NMR techniques for studying metal phosphine complexes in the solid state, Organometallics 11 (1992) 3242–3248.
[50] C. Merckle, J. Bluemel, Improved rhodium hydrogenation catalysts immobilized on silica, Top. Catal. 34 (2005) 5–15.
[51] B. Beele, J. Guenther, M. Perera, M. Stach, T. Oeser, Bluemel, New linker systems for superior immobilized catalysts, J. New J. Chem. 34 (2010) 2729–2731.
[52] M. Carvalho, L.F. Wieserman, D.M. Hercules, Spectroscopic characterization of Wilkinson's catalyst using X-ray photoelectron spectroscopy (ESCA), Appl. Spectrosc. 36 (1982) 290–296.
[53] R. Yerushalmi, J.C. Ho, Z.-Y. Fan, A. Javey, Phosphine oxide monolayers on SiO_2 surfaces, Angew. Chem. Int. Ed. 47 (2008) 4440–4442.
[54] R.K. Blundell, P. Licence, Quaternary ammonium and phosphonium based ionic liquids: a comparison of common anions, Phys. Chem. Chem. Phys. 16 (2014) 15278–15288.
[55] P. Li, S. Kawi, SBA-15-based polyamidoamine dendrimer tethered Wilkinson's rhodium complex for hydroformylation of styrene, J. Catal. 257 (2008) 23–31.
[56] A. Sabarre, Love, Synthesis of 1,1-disubstituted olefins via catalytic alkyne hydrothiolation/Kumada cross-coupling, J. Org. Lett. 10 (2008) 3941–3944.
[57] A. Di Giuseppe, R. Castarlenas, J.J. Pere-Torrente, M. Crucianelli, V. Polo, R. Sancho, F.J. Lahoz, L.A. Oro, Ligand-controlled regioselectivity in the hydrothiolation of alkynes by rhodium N-heterocyclic carbene catalysts, J. Am. Chem. Soc. 134 (2012) 8171–8183.
[58] H. Zhao, J. Peng, M.Z. Cai, Heterogeneous hydrothiolation of alkynes with thiols catalyzed by diphosphino-functionalized MCM-41 anchored rhodium complex, Catal. Lett. 142 (2012) 138–142.
[59] C. Cao, L.R. Fraser, J.A. Love, Rhodium-catalyzed alkyne hydrothiolation with aromatic and aliphatic thiols, J. Am. Chem. Soc. 127 (2005) 17614–17615.
[60] Y. Misumi, H. Seino, Y. Mizobe, Addition of benzenethiol to terminal alkynes catalyzed by hydrotris(3,5-dimethylpyrazolyl)borate-Rh(III) bis(thiolate) complex: mechanistic studies with characterization of the key intermediate, J. Organomet. Chem. 691 (2006) 3157–3164.
[61] A. Ogawa, T. Ikeda, K. Kimura, T. Hirao, Highly regio-and stereocontrolled synthesis of vinyl sulfides via transition-metal-catalyzed hydrothiolation of alkynes with thiols, J. Am. Chem. Soc. 121 (1999) 5108–5114.
[62] L.D. Field, B.A. Messerle, K.Q. Vuong, P. Turner, Rhodium (I) and iridium (I) complexes containing bidentate phosphine-imidazolyl donor ligands as catalysts for the hydroamination and hydrothiolation of alkynes, Dalton Trans. 3599–3614 (2009).
[63] V.P. Ananikov, K.A. Gayduk, N.V. Orlov, I.P. Beletskaya, V.N. Khrustalev, M.Y. Antipin, Two distinct mechanisms of alkyne insertion into the metal-sulfur bond: combined experimental and theoretical study and application in catalysis, Chem. Eur. J. 16 (2010) 2063–2071.
[64] V.P. Ananikov, N.V. Orlov, I.P. Beletskaya, Efficient and convenient synthesis of β-vinyl sulfides in nickel-catalyzed regioselective addition of thiols to terminal alkynes under solvent-free conditions, Organometallics 25 (2006) 1970–1977.
[65] S.N. Riduan, J.Y. Ying, Y.G. Zhang, Carbon dioxide mediated stereoselective copper-catalyzed reductive coupling of alkynes and thiols, Org. Lett. 14 (2012) 1780–1783.
[66] S. Ranjit, Z. Duan, P. Zhang, X.-G. Liu, Synthesis of vinyl sulfides by copper-catalyzed decarboxylative C-S cross-coupling, Org. Lett. 12 (2010) 4134–4136.
[67] V.P. Ananikov, N.V. Orlov, I.P. Beletskaya, V.N. Khrustalev, M.Y. Antipin, T.V. Timofeeva, New approach for size-and shape-controlled preparation of Pd nanoparticles with organic ligands. Synthesis and application in catalysis, J. Am. Chem. Soc. 129 (2007) 7252–7253.
[68] H. Kuniyasu, A. Ogawa, K. Sato, I. Ryu, N. Kambe, N. Sonoda, The first example of transition-metal-catalyzed addition of aromatic thiols to acetylenes, J. Am. Chem. Soc. 114 (1992) 5902–5903.
[69] I.P. Beletskaya, V.P. Ananikov, Addition reactions of EE and EH bonds to triple bond of alkynes catalyzed by Pd, Pt, and Ni complexes (E= S, Se), Pure Appl. Chem. 79 (2007) 1041–1056.
[70] A. Corma, C. Gonzalez-Arellano, M. Iglesias, F. Sanchez, Efficient synthesis of vinyl and alkyl sulfides via hydrothiolation of alkynes and electron-deficient olefins using soluble and heterogenized gold complexes catalysts, Appl. Catal., A 375 (2010) 49–54.
[71] C.J. Weiss, T.J. Marks, Organozirconium complexes as catalysts for Markovnikov-selective intermolecular hydrothiolation of terminal alkynes: scope and mechanism, J. Am. Chem. Soc. 132 (2010) 10533–10546.
[72] C.J. Weiss, S.D. Wobser, T.J. Marks, Organoactinide-mediated hydrothiolation of terminal alkynes with aliphatic, aromatic, and benzylic thiols, J. Am. Chem. Soc. 131 (2009) 2062–2063.
[73] C.J. Weiss, S.D. Wobser, T. Marks, Lanthanide-and actinide-mediated terminal alkyne hydrothiolation for the catalytic synthesis of Markovnikov vinyl sulfides, Organometallics 29 (2010) 6308–6320.
[74] K.Q. Vuong, Ph.D. Thesis, University of New South Wales, Australia, 2006.
[75] I. Ojima, N. Clos, R.J. Donovan, P. Ingallina, Organometallics 9 (1990) 3127–3133.
[76] B.M. Trost, Z.T. Ball, Alkyne hydrosilylation catalyzed by a cationic ruthenium complex: efficient and general trans addition, J. Am. Chem. Soc. 127 (2005) 17644–17655.
[77] T. Hirabayashi, Y. Okimoto, A. Saito, M. Morita, S. Sakaguchi, Y. Ishii, Total synthesis of (±)-herbertenediol, Tetrahedron 62 (2006) 2–4.
[78] R. Casado, M. Contel, M. Laguna, P. Romero, S. Sanz, Organometallic gold (III) compounds as catalysts for the addition of water and methanol to terminal alkynes, J. Am. Chem. Soc. 125 (2003) 11925–11935.
[79] E. Mizushima, K. Sato, T. Hayashi, M. Tanaka, Highly efficient AuI-catalyzed hydration of alkynes, Angew. Chem., Int. Ed. 41 (2002) 4563–4565.
[80] D.B. Grotjahn, D.A. Lev, A general bifunctional catalyst for the anti-Markovnikov hydration of terminal alkynes to aldehydes gives enzyme-like rate and selectivity enhancements, J. Am. Chem. Soc. 126 (2004) 12232–12233.
[81] X. Jin, T. Oishi, K. Yamaguchi, N. Mizuno, Heterogeneously catalyzed efficient hydration of alkynes to ketones by tin–tungsten mixed oxides, Chem. Eur. J. 17 (2011) 1261–1267.

[82] M. Kondo, T. Kochi, F. Kakiuchi, Rhodium-catalyzed anti-Markovnikov intermolecular hydroalkoxylation of terminal acetylenes, J. Am. Chem. Soc. 133 (2011) 32–34.
[83] Muzart, Gold-catalysed reactions of alcohols: isomerisation, inter-and intramolecular reactions leading to C-C and C-heteroatom bonds, J. Tetrahedron 64 (2008) 5815–5849.
[84] J.H. Teles, S. Brode, M. Chabanas, Cationic gold(I) complexes: highly efficient catalysts for the addition of alcohols to alkynes, Angew. Chem., Int. Ed. 37 (1998) 1415–1418.
[85] M. Bouhrara, E. Jeanneau, L. Veyre, C. Coperet, C. Thieuleux, Dissymmetric gold(I) N-heterocyclic carbene complexes: a key unexpected structural parameter for highly efficient catalysts in the addition of alcohols to internal alkynes, Dalton Trans. 40 (2011) 2995–2999.
[86] L.-Z. Dai, M.-J. Qi, Y.-L. Shi, X.-G. Liu, M. Shi, Gold (I)-Catalyzed cascade cyclization reaction: highly regio-and diastereoselective intermolecular addition of water and alcohols to epoxy alkynes, Org. Lett. 9 (2007) 3191–3194.
[87] J.W. Hartman, L. Sperry, Platinum (II)-catalyzed addition of alcohols to alkynes, Tetrahedron Lett. 45 (2004) 3787–3788.
[88] T.E. Müller, K.C. Hultzsch, M. Yus, F. Foubelo, M. Tada, Hydroamination: direct addition of amines to alkenes and alkynes, Chem. Rev. 108 (2008) 3795–3892.
[89] K.D. Hesp, M. Stradiotto, Stereo-and regioselective gold-catalyzed hydroamination of internal alkynes with dialkylamines, J. Am. Chem. Soc. 132 (2010) 18026–18029.
[90] M. Tokunaga, M. Eckert, Y. Wakatsuki, Ruthenium-catalyzed intermolecular hydroamination of terminal alkynes with anilines: a practical synthesis of aromatic ketimines, Angew. Chem., Int. Ed. 38 (1999) 3222–3225.
[91] F. Pohlki, S. Doye, The catalytic hydroamination of alkynes, Chem. Soc. Rev. 32 (2003) 104–114.
[92] E. Mizushima, T. Hayashi, M. Tanaka, Au (I)-catalyzed highly efficient intermolecular hydroamination of alkynes, Org. Lett. 5 (2003) 3349–3352.
[93] C.G. Hartung, A. Tillack, H. Trauthwein, M. Beller, A convenient rhodium-catalyzed intermolecular hydroamination procedure for terminal alkynes, J. Org. Chem. 66 (2001) 6339–6343.
[94] S. Burling, L.D. Field, B.A. Messerle, Hydroamination of alkynes catalyzed by a cationic rhodium (I) complex, Organometallics 19 (2000) 87–90.
[95] L.M. Lutete, I. Kadota, Y. Yamamoto, Palladium-catalyzed intramolecular asymmetric hydroamination of alkynes, J. Am. Chem. Soc. 126 (2004) 1622–1623.
[96] H.W. Cheung, C.M. So, K.H. Pun, Z. Zhou, C.P. Lau, Hydro(trispyrazolyl)borato-ruthenium(II) diphosphinoamino complex-catalyzed addition of β-Diketones to 1-alkynes and anti-Markovnikov addition of secondary amines to aromatic 1-alkynes, Adv. Synth. Catal. 353 (2011) 411–425.
[97] Y. Fukumoto, T. Kawahara, Y. Kanazawa, N. Chatani, Synthesis of (E)-3-alkylidene-1-pyrrolines by the rhodium-catalyzed cyclization of terminal alkynes with homopropargylic amines, Adv. Synth. Catal. 351 (2009) 2315–2318.
[98] S. Burling, L.D. Field, B.A. Messerle, K.Q. Vuong, P. Turner, Rhodium (I) and iridium (I) complexes with bidentate N, N and P, N ligands as catalysts for the hydrothiolation of alkynes, Dalton Trans. (2003) 4181–4191.
[99] M. Arisawa, K. Fujimoto, S. Morinaka, M. Yamaguchi, Equilibrating C-S bond formation by C-H and S-S bond metathesis: rhodium-catalyzed alkylthiolation reaction of 1-alkynes with disulfides, J. Am. Chem. Soc. 127 (2005) 12226–12227.
[100] A. Lumbroso, N.R. Vautravers, B. Breit, Rhodium-catalyzed selective anti-Markovnikov addition of carboxylic acids to alkynes, Org. Lett. 12 (2010) 5498–5501.
[101] A. Lumbroso, P. Koschker, N.R. Vautravers, B. Breit, Redox-neutral atom-economic rhodium-catalyzed coupling of terminal alkynes with carboxylic acids toward branched allylic esters, J. Am. Chem. Soc. 133 (2011) 2386–2389.
[102] M. Nishiumi, H. Miura, K. Wada, S. Hosokawa, M. Inoue, Recyclable solid ruthenium catalysts supported on metal oxides for the addition of carboxylic acids to terminal alkynes, Adv. Synth. Catal. 352 (2010) 3045–3052.
[103] C.S. Yi, R. Gao, Scope and mechanistic investigations on the solvent-controlled regio- and stereoselective formation of enol esters from the ruthenium-catalyzed coupling reaction of terminal alkynes and carboxylic acids, Organometallics 28 (2009) 6585–6592.
[104] D.-M. Cui, Q. Meng, J.-Z. Zheng, C. Zhang, Gold-catalyzed addition of sulfonic acids to alkynes to form vinyl sulfonates, Chem. Commun. 1577–1579 (2009).
[105] A.V. Vasilyev, S. Walspurger, S. Chassaing, P. Pale, J. Sommer, One-step addition of sulfonic acids to acetylene derivatives: an alternative and stereoselective approach to vinyl triflates and fluorosulfonates, Eur. J. Org. Chem. 5740–5748 (2007).
[106] Y. Yang, E.G. Moschetta, R.M. Rioux, Addition of sulfonic acids to terminal alkynes catalyzed by a rhodium complex: ligand concentration-controlled reaction selectivity, ChemCatChem. 10 (2013) 3005–3013.
[107] W.M. Jones, D.D. Maness, Solvolysis of sulfonic acid esters of triphenylvinyl alcohol by a heterolytic mechanism, J. Am. Chem. Soc. 91 (1969) 4314–4315.
[108] P.J. Stang, R. Summerville, Solvolysis of sulfonic acid esters of triphenylvinyl alcohol by a heterolytic mechanism, J. Am. Chem. Soc. 91 (1969) 4600–4601.
[109] M.A. Garcia, M. Hanack, R.H. Summerville, P.V.R. Schleyer, P.J. Stang, 1-tert-Butylvinyl trifluoromethanesulfonate: solvolysis and rearrangement via a vinyl cation, Angew. Chem., Int. Ed. Engl. 9 (1970) 302–303.
[110] P.J. Stang, T.E. Fisk, Single-step improved synthesis of primary and other vinyl trifluoromethanesulfonates, Synthesis (1979) 438–440.
[111] P.J. Stang, W. Treptow, Single-step improved synthesis of primary and other vinyl trifluoromethanesulfonates, Synthesis (1980) 283–284.